



# Efficiency Improvement of Non-crystal Silicon (Amorphous) Photovoltaic Module in a Solar Hybrid System with Nanofluid

H. Asadian<sup>1</sup> · A. Mahdavi<sup>1</sup> · T.B. Gorji<sup>2</sup> · M. Gorji-Bandpy<sup>1</sup>

Received: 6 November 2020 / Accepted: 24 July 2021 / Published online: 10 August 2021  
© The Society for Experimental Mechanics, Inc 2021

## Abstract

The significance of solar energy among renewable energy resources is undeniable and its benefits are well known. However, due to its intermittent nature and the relatively low efficiency of solar systems, it supplies only a small percentage (i.e., <1%) of the world's energy. Second-generation photovoltaic modules-devices that can convert solar radiation into electricity offer low efficiency (<13.4%), and a large amount of energy in these devices is wasted in the form of heat. This study investigated a hybrid system that can utilize such wasted thermal energy from a photovoltaic module. These systems, known as photovoltaic-thermal (PVT) hybrid systems, can harness solar energy in the form of heat and electricity. The performance of PVT hybrid systems is experimentally studied, and water, considered as the working fluid, is moved through serpentine tubes mounted at the back of the PV module. Furthermore, to enhance the thermophysical properties of the working fluid, various nanoparticles (TiO<sub>2</sub>, SiO<sub>2</sub>, and C) are added to the base fluid. The results indicate that using PVT/w with copper tubes can elevate the thermal efficiency up to 89.11% and electrical efficiency increases by almost 0.6%. During the nanofluids tests, the highest increase of 24.15% in thermal efficiency was observed by using graphite nanofluids.

**Keywords** Solar energy · Photovoltaic module · Electrical and thermal efficiencies · Photovoltaic thermal hybrid system (PVT) · Nanofluid

## Introduction

Solar energy can be generally harnessed for two main purposes: 1) to generate heat, which is performed in solar thermal collectors, 2) to generate electricity, which can be carried out by photovoltaic modules. Photovoltaic modules have very low efficiency and electrical efficiency reduces when module temperature increases [1–3]. A large quantity of energy in these devices is wasted in the form of heat which can be reused for water heating applications. Therefore, a hybrid system called Photovoltaic-Thermal (PVT) is considered for this study, catering for both heating and power generating simultaneously. Thus, the total efficiency of the Photovoltaic

modules can be increased to a larger extent as a result of cooling operation, which reduces the overall module temperature, leading to better module efficiency and longer longevity. PVT systems are usually categorized according to their operating fluid. Many of them employ air as the working fluid while others use water. Based on the selection of working fluid, the systems are called PVT/a and PVT/w for air and water, respectively. In this study, PVT/w is considered.

Wolf [4] and Florschuetz [5] carried out pioneering works on PVT systems using PVT/a. However, the first important study on PVT/w was done by Prakash in 1994 [6]. He used a simple PVT system that applied air and water flow. The PVT/a system acquired efficiency between 17%–51%, and for PVT/w an efficiency of 50%–67% was achieved in different flow rates. Tripanagnostopoulos et al. [7] compared different PVT systems economically and concluded that PVT/a system is about 5% more expensive than the PV modules. According to their empirical experiments, and by improvements which they have made, the PVT/a thermal efficiency was about 38–75% and for PVT/w systems was about 55–85%.

✉ A. Mahdavi  
arashmahdavi93@gmail.com

<sup>1</sup> Department of Mechanical Engineering, Babol Noshirvani University of Technology, Babol, Iran

<sup>2</sup> Department of Mechanical Engineering, Mazandaran Institute of Technology, Babol, Iran

Zondag et al. [8, 9] after examining different PVT/w systems, concluded that using a glass cover on the solar module would increase the thermal efficiency up to 6%. An analytical study has been carried out to predict the temperature of hot water output of a PVT/w system by Tiwari et al. [10], and it was concluded that thermal efficiency increases by increasing mass flow rate, however, this will result in temperature drop within the thermal collector. One of the important applications of PVT/w systems is their combination with thermal pumps and thermal systems. In this regard, studies have been carried out which are considered as examples of integrated photovoltaic-thermal systems such as Kalogirou [11], Kalogirou and Tripanagnostopoulos [12] and Chow et al. [13].

The effect of applying nanofluids on the performance of photovoltaic thermal (PV/T) systems has been studied by various researchers during recent years and it can be generally conjectured that the best method to enhance the thermal efficiency of a solar PVT system is the utilization of nanofluids [14], especially nanofluids with higher thermal conductivity significantly enhance the performance of solar PV/T systems [15–18].

Based on a review of the available literature, there has been no experimental research on PVT systems with amorphous modules using nanofluids. In the present study, a thin layer non-crystal silicon (amorphous) solar module has been selected for experimental assessment. By the combination of solar module with tube-type thermal collectors which are made of aluminum or copper, a PVT/w system is investigated. In this research, various types of nanofluids have been analyzed, some of which are experimentally used for the first time in this field and have been very effective in PVT/w system cooling, resulting in a remarkable enhancement in PVT/w system efficiency.

## Definitions and Concepts

The electrical efficiency of solar energy conversion is an important parameter to assess the performance of photovoltaic modules in the photovoltaic (PV) and PVT systems. Using I-V diagrams, the maximum output power is determined by the current and voltage at the maximum power point ( $I_{MP}$ ). Figure 1 shows the I-V diagram and the P-V diagram for conventional photovoltaic modules.

As a result, the electrical efficiency of a photovoltaic module ( $\eta_e$ ) can be calculated as follows [20]:

$$\eta_e = \frac{I_{mp} \times V_{mp}}{G \times A_c} \quad (1)$$

where “ $G$ ” is the amount of radiation entering the solar module and “ $A_c$ ” is the area of the solar module. In a PVT system, the amount of electrical efficiency will be slightly higher than an equivalent PV, due to fluid cooling. By measuring the inlet

and outlet temperature of the fluid used in the PVT system (which is water in this test), the thermal efficiency of the system can be calculated according to the following equation [20]:

$$\eta_{th} = \frac{\dot{m} \times C \times (T_{out} - T_{in})}{G \times A_c} \quad (2)$$

Where “ $\dot{m}$ ” is the mass flow rate and “ $C$ ” is the specific heat capacity. When using nanofluids, these parameters are required to be modified accordingly. The total efficiency of PVT systems is as follows:

$$\eta_{tot} = \eta_e + \eta_{th} \quad (3)$$

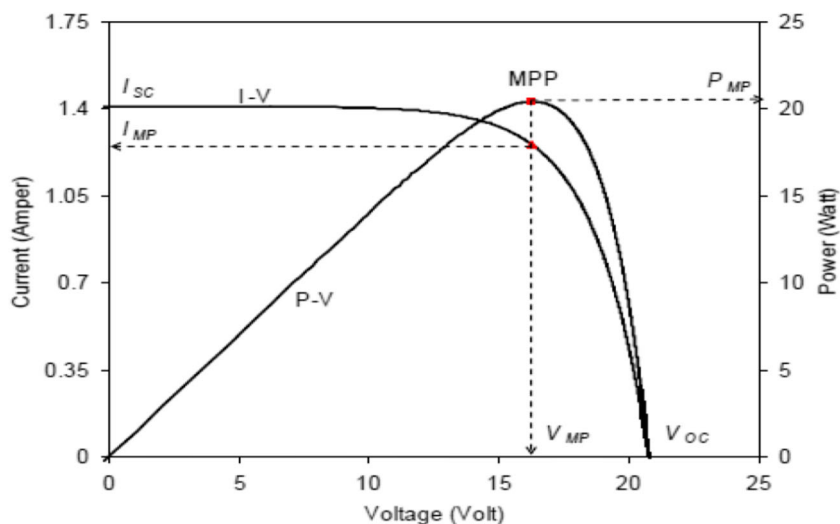
The use of nanofluids in PVT/w systems can greatly enhance the thermal efficiency. Nanofluids, which are produced from the distribution of nano-sized particles in conventional fluids, are a new generation of fluids with great potential in industrial applications. The idea of nanofluid was developed by Choi and Eastman, pioneering nanofluid applications in thermo-fluids science [21]. The particle size used in nanofluids is from 1 nm to 100 nm. Nano-fluids generally have high thermal conductivity and hence their heat transfer rate is very high. One of the important issues to be considered in the preparation of nanofluids is the stability of nanofluids. Nanofluids are not a simple mixture of liquid and solid particles, while nanoparticles tend to be agglomerated due to high levels of activity and this agglomeration may change the physical properties of the nanofluid. The most important factors affecting the stability of nanofluids include: concentration of nanoparticles, fluid viscosity, pH, type of nanoparticles, nanoparticles diameter and ultrasonic time [22]. One of the best methods for increasing the stability of nanofluids is the addition of a surfactant. Furthermore, it has been reported that the addition of surfactants can increase the stability of the nanofluids at higher temperature rates [14]. In this research, sodium dodecyl sulfate (SDS) surfactant is added to avoid agglomeration and increase the stability of the prepared nanofluids.

In this experiment, nanofluid mixtures at 0.1% concentration were used. The correlation Eq. (4) below represents nanofluid concentration [23]:

$$\phi = \frac{\frac{m_{nano}}{\rho_{nano}}}{\frac{m_{nano}}{\rho_{nano}} + \frac{m_{bf}}{\rho_{bf}}}$$

Where “ $m$ ” and “ $\rho$ ” refer to the mass and density respectively. The total value of “ $\frac{m_{bf}}{\rho_{bf}}$ ” represents the volume of the fluid container used to dissolve the nanofluid particles. This amount is 250 ml for the mixture of water and SDS (SDS, 30.0 wt%) in this experiment. As an example, for a 0.1%

**Fig. 1** I-V and the P-V diagrams for conventional Photovoltaic modules [19]



concentration, the amount of nanoparticles required by the above equation is obtained as follows:

$$m_{SiO_2} = 0.549 \text{ gr}, \quad m_{TiO_2} = 1.124 \text{ gr}, \quad m_C = 0.556 \text{ gr} \quad (5)$$

In Fig. 2, the nanoparticles used in the system with the surfactant (SDS) are shown.

## Experimental Approach

Initially, in order to conduct the experiment, a solar module made of thin-layer non-crystal silicon (amorphous) was selected. Amorphous modules are cheaper than crystalline silicon modules, and their capability in compensating the energy loss in the form of heat make them a suitable candidate, despite their lower efficiency. On the other hand, because of the more favorable price of these modules, and also their capability to capture longer wavelengths, a promising future for the practical application of these modules could be expected. The amorphous module used for this research is shown in Fig. 3. This module is a product of Conrad Electronic of 12 Volt, 4 W ultimate power and the surface area is  $31.5 \times 31.5 \text{ cm}^2$ . The operating temperature range for the module is between  $-40^\circ \text{C}$  to  $80^\circ \text{C}$ . Other technical data related to this module is provided in Table 1.

A type of solar simulator was developed to provide the light and heat needed for this test, which uses a metal-halide HQI-T lamp with a color temperature of 5500 K similar to the AM1.5 solar spectrum to simulate the solar spectrum (Fig. 4).

The thermal collector used in the system is a serpentine tube-plate type that connects either aluminum or copper tubes to an aluminum sheet which has a thickness of one millimeter. Since PVT/w systems, thermal collectors are simply made and employed; This simplicity makes the solar collector easier to be installed on the back of the solar module, and in general less space will be occupied. There are several methods for connecting aluminum or copper tubes to the aluminum sheet (mounted at the backside of the module), which include two methods of welding and bonding through heat conductive adhesives. In this test, bonding was more convenient because of the low surface area of the solar module and the small thickness of the aluminum sheet. Besides, not only the welding method has a higher cost, but also it may damage or warp the aluminum sheet and thus damages the solar module. The arrangement of these serpentine tubes on the aluminum sheet is very important, which may be affected by parameters such as low module surface area, back panel geometry of the module and the number of serpentine tube turns. Based on the results of previous experiments [8, 9], and the low space available at the backside solar modules, as well as the rapid heat transfer rate, the method of winding serpentine tubes is an

**Fig. 2** Nanoparticle samples  $TiO_2$ ,  $SiO_2$ , C and surfactant (SDS)



**Table 1** Characteristics of the selected PV module in this experimental study

Short-circuit current	320 mA
No-load voltage	21 V
Power output	4 W
Rated voltage	17.5 V
Rated current	230 mA
Weight	1.56 kg
Dimensions ( $W \times H \times D$ )	315 × 315 × 19 mm

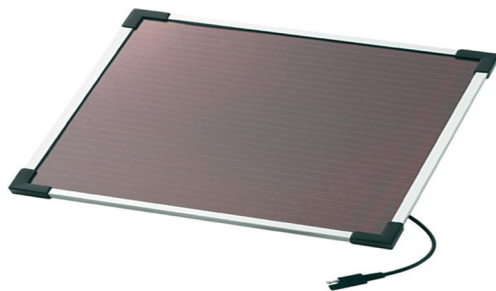
appropriate method. The number of turns of the serpentine tubes was empirically determined, then the entire set of tubes was mounted on the backside of the module and finally the surrounding area was thoroughly insulated, which was very effective in preventing heat dissipation. In Fig. 5, thermal collector tubes and the final insulated system are shown.

While a potentiometer was employed to control the voltage of the electrical circuit; a rheostat was used to monitor the flow of current within the circuit at different resistances.

In order to ensure stability, the nanofluids have been prepared via a two-step preparation method which involves 30–45 min of mixing of nanoparticles in 0.1% volume fraction into the base fluid (over 3 periods of 10 to 15 min) in a bath type ultrasonicator (Sonica S3 by Soltec shown in Fig. 6a). Using low volume fractions of nanoparticles (i.e. 0.1% vol.) guarantees higher stability over time [25]. The prepared nanofluids mixtures did not exhibit any visible sedimentation issues after being left at room temperature for two weeks.

Solar radiation intensity was measured and recorded using a TES-1333R solar power meter, with an accuracy of  $\pm 5\%$ . This accuracy was stated in accordance with the manufacturer's catalog.

To measure the voltage and output current of the solar module and also for measuring the temperature of the photovoltaic module and the temperature of the inlet and outlet of the fluid (or nanofluid), a DEC-330FC multimeter was used, which is powered by a direct-current voltage system, since the output current of the photovoltaic system is direct current. The DEC-330FC has a range of temperatures ranging from  $-20$  to  $+1000^\circ\text{C}$ . The temperature probe is calibrated by placing it in

**Fig. 3** Thin-layer non-crystal (amorphous) photovoltaic module

a controlled temperature bath at  $100^\circ\text{C}$  (boiling water) and  $0^\circ\text{C}$  (ice and water mixture). By comparing the achieved temperatures with a Zeal L0161 mercury thermometer, the uncertainty value was obtained at  $\pm 1\%$ .

In the experiments, a BT100-2 J Longer peristaltic pump is used to drive the cooling fluid. Peristaltic pumps have the advantage of transferring corrosive fluids or a fluid with abrasive particles into a tube without any contact with other parts of the pump (Fig. 6c).

Another advantage of these pumps is the measurement of the fluid flow rate by the pump itself, which requires a calibration of the discharge measured by the pump [26]. The volumetric flow rate in a peristaltic pump can be measured as follows:

$$Q = \alpha \cdot rpm \quad (6)$$

In the above equation, “rpm” is the number of pump rounds per minute and “ $\alpha$ ” is the specific measurement coefficient of the peristaltic pump. To measure the discharge rate of the pump, it is necessary to measure the coefficient “ $\alpha$ ”. First, a 250 ml container was selected and the filling time was measured during different “rpm” values. At each “rpm”, the filling time of the container was measured 10 times repeatedly, so as to obtain an average value. Therefore:

$$Q = \frac{V}{t_{av}} \quad (7)$$

where “V” is the volume of the container and “ $t_{av}$ ” is the mean-time of filling the container. With the help of the above relation, the value of “Q” in each particular “rpm” can be calculated and, by inserting in eq. (6), the value of the coefficient “ $\alpha$ ” in each particular “rpm” is achieved. By averaging them, “ $\alpha_{av}$ ” value for this experiment ( $\alpha_{av} = 0.03307 \frac{\text{ml}}{\text{sec} \cdot \text{rpm}}$ ) was gained.

After all, this value should be used for “ $\alpha$ ” in eq. (6). The uncertainty value obtained for this test is about  $\pm 1.43\%$ . With the constant value for “ $\alpha_{av}$ ” determined by eq. (6), the flow rate in terms of “rpm” variations could be expressed.

In this study, initially, the electrical efficiency of the amorphous module (PV system only) was measured at different radiation intensities. In order to calculate the maximum electrical efficiency, there are different theoretical and practical approaches, some of which are used only for certain types of modules and during specific states. However, the best method in practical applications is to use trial and error. According to the I-V and P-V diagrams of the solar modules, the maximum power of each module can be calculated. First, the electrical current and voltage values at different resistance values were required, then, using the interpolation method, the maximum yield range was determined. The maximum yield value can be obtained by performing further experiments.

Then, the same method was utilized on the PVT/w system to calculate its electrical efficiency. By measuring the water temperature at the inlet and outlet of the PVT/w system, the



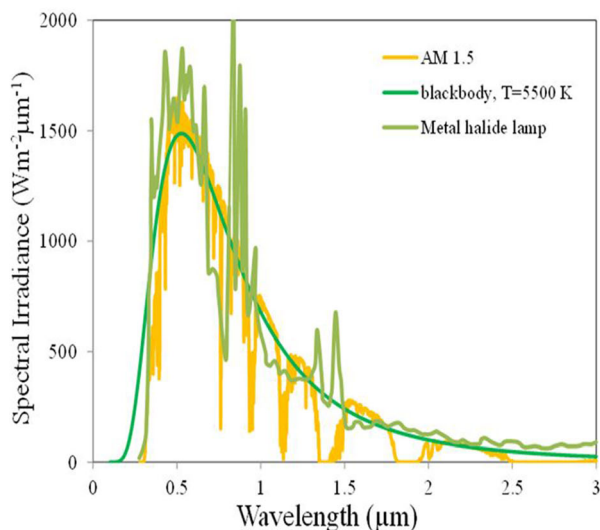


Fig. 4 Solar spectrum simulator [24]

thermal efficiency of the system can also be calculated. By changing the flow rate of the inlet fluid, the effect of this parameter on the cooling of the module and the amount of thermal and electrical efficiencies were calculated.

The next step is to use a variety of nanofluids that can greatly enhance the thermal efficiency of the system. The results can be compared with a PVT/w system without nanofluid and a sole PV system. In Fig. 7, an overview of the PVT/w complete setup is shown.

### Results and Discussion

In order to obtain the efficiency of a photovoltaic module at different radiation intensities, it is necessary first to

draw up an I-V diagram (by varying the resistance value and obtaining the values of I and V). The area under the I-V curve represents the amount of electrical power output of the photovoltaic module, and consequently, the P-V diagram can be plotted. From Fig. 8 it can be concluded that as the radiation intensity is amplified the maximum point of the P-V curve is elevated. Looking at the I-V diagram, it is noteworthy to mention that the amount of open-circuit voltage increases slightly with raising the intensity of the incoming radiation. Although, with the intensity surging upward, the short circuit current is significantly increased initially, the slope of the short-circuit current tends to plateau at higher intensities. In Fig. 8 I-V and P-V diagrams are plotted at different radiation intensities respectively.

Fig. 5 Thermal collector tubes and the final insulated system

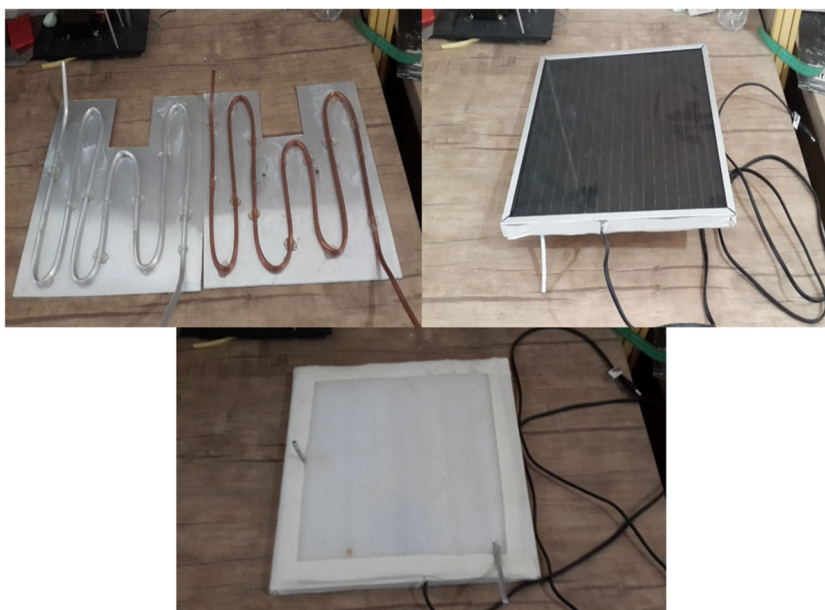


**Fig. 6** a) Sonica ultrasonic device, b) TES 1333 Solar Power Meter, c) Peristaltic Pump



Figure 9 shows the electrical efficiency of the module versus radiation intensity which is obtained by eq. (1). Obviously, as the radiation intensity increases, the module temperature is increased. Therefore, the electrical output power is enhanced, however, this will reduce the module’s electrical efficiency due to the higher temperature. In general, the electrical efficiency of amorphous modules is very low in practical applications, hence, they are not suitable for domestic or industrial applications. Nevertheless, they can be very useful for PVT/w systems.

In Fig. 10, the results of I-V and P-V characteristic curves during different radiation intensities are demonstrated. The plots are obtained from experiments with aluminum serpentine tubes, at a given flow rate. In order to setup this test, “rpm = 6” is adjusted for peristaltic pump so that providing a constant flow rate. The results obtained for the I-V and P-V diagrams show that the electrical efficiency increases at low radiation intensity due to the higher cooling effect during lower isolations. However, during higher intensities, the efficiency increasing rate will be milder, which means the electrical

efficiency of the PVT/w system will not vary significantly, compared to the same state of a sole PV module. The reason is due to the inner structure of the solar modules, which, even with cooling, does not have the potential to increase electrical efficiency. Not only amorphous modules but also other sorts of modules have structural weaknesses to enhance electrical efficiency (especially at high radiation levels). In order to determine the reduction of efficiency increment process at high



**Fig. 7** PVT/w system overview with peripheral equipment

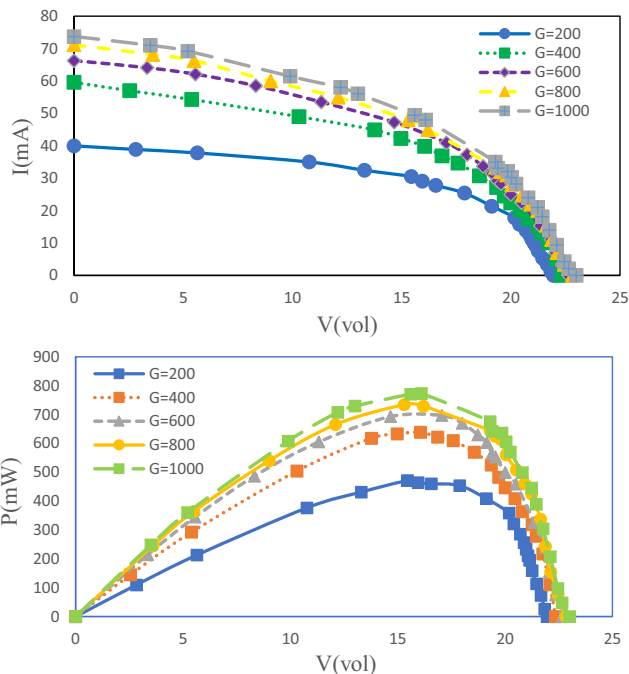


**Fig. 8** I-V and P-V diagrams in different radiation intensities for PV system

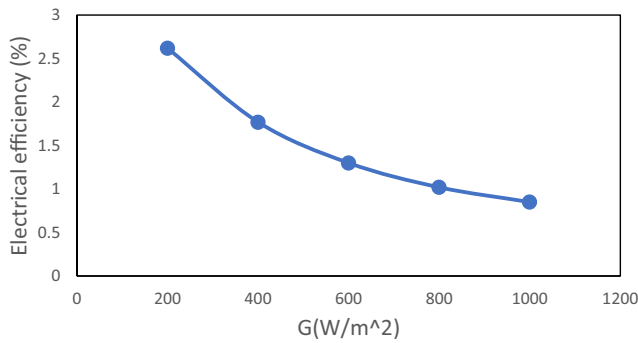


Fig. 9 PV system electrical efficiency in different radiation intensities

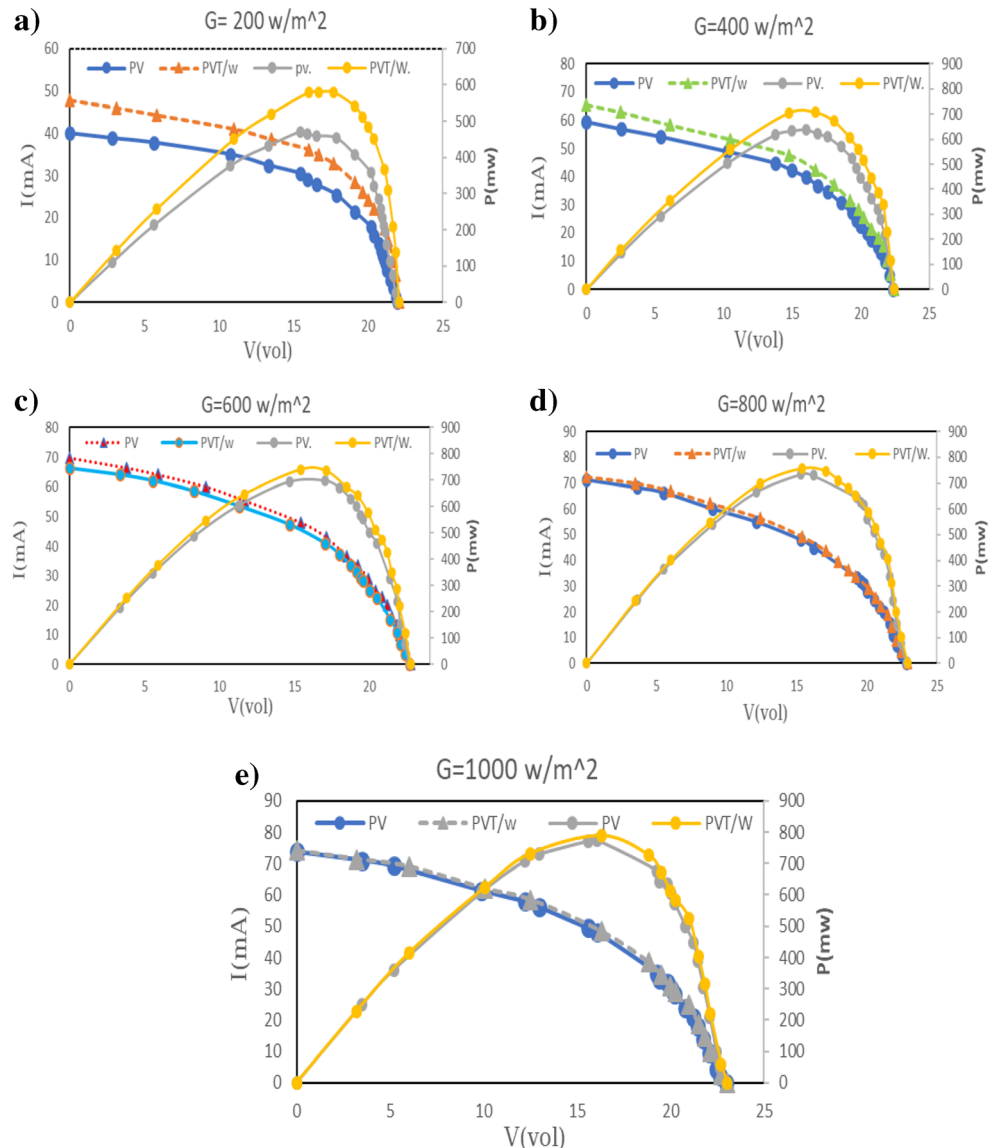
radiation intensity, each radiation intensity is shown in a separate curve, the same trend is observed for the P-V chart.

A change in fluid flow rate (or change in  $rpm$ ) can also affect the electrical efficiency of the PVT/w system. Although enhancing the flow rate will increase the electrical

efficiency, the resulting enhancement is not proportionately significant. In Fig. 11, the I-V and P-V diagrams of the PVT/w system with an aluminum tube at a constant radiation intensity ( $G = 600 \frac{W}{m^2}$ ) are compared in different rounds of the pump ( $rpm = 6, 8$  and  $10$ ), indicating that the curves are very close to each other.

By utilizing copper serpentine tubes instead of aluminum tubes, a significant effect on the thermal performance of PVT/w systems was achieved which is due to the higher thermal conductivity of copper. Although the use of copper tubes will slightly increase the electrical efficiency of the PVT/w system, the effect of using it is not significant (the amount of this change in the electrical efficiency is indicated in the next section). From Fig. 12 it can be conjectured that the I-V and P-V diagrams of PVT/w with copper and aluminum tubes have similar trends.

Fig. 10 I-V and P-V diagrams for Comparison between PVT/W and PV systems during different radiation intensities a) 200, b) 400, c) 600, d) 800, e) 1000  $W/m^2$



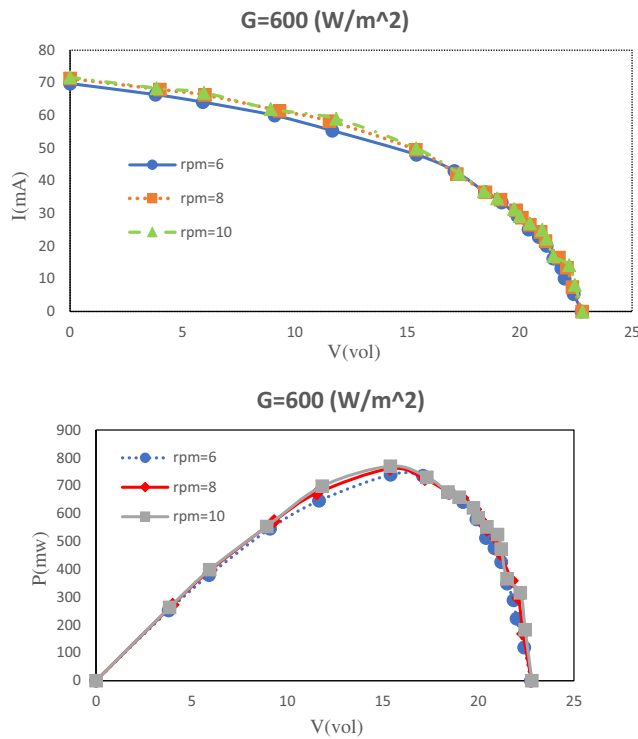


**Fig. 11** I-V and P-V diagrams of PVT/w system at a constant radiation intensity ( $G = 600 \frac{W}{m^2}$ ) and during different pump rotation speeds

Now the electrical efficiency of PVT/w system can be calculated. In Fig. 13, the electrical efficiency in two modes of aluminum and copper serpentine tubes with  $rpm = 6$ , are compared to a conventional photovoltaic module (PV).

As shown in Fig. 13, the diagrams related to the two setups that use copper and aluminum serpentine tubes are very close to each other and as expressed before, tube material type was not remarkably effective in electrical efficiency. However, compared to a conventional photovoltaic system, the difference in electrical efficiency is greater for the case of lower radiation intensities, and the efficiency of the three systems was approximately the same at high radiation intensities. For example, at the radiation of  $G = 200 \frac{W}{m^2}$ , the value obtained for the photovoltaic module electrical efficiency is 2.62%, which

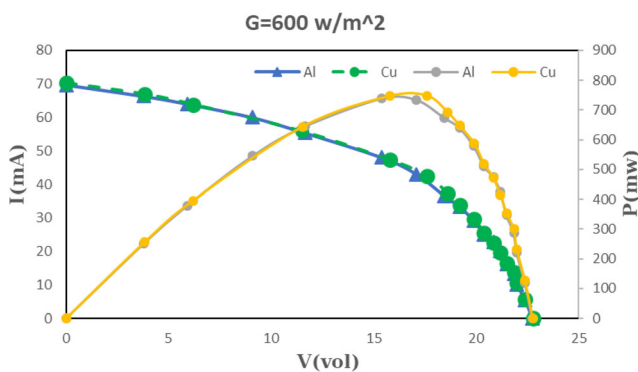


**Fig. 12** I-V and P-V diagrams of PVT/w with copper and aluminum tubes in  $rpm = 6$  and  $G = 600 \frac{W}{m^2}$

is approximately 3.22% for the aluminum tube in PVT/w system and 3.26% for copper tube mode. This increase in electrical efficiency seems to be negligible, and in general research on all types of solar modules, a maximum of 1 to 2% increase in electrical efficiency (using a photovoltaic-thermal cooling system) has been observed.

Water is a substance that has a high specific heat capacity and its specific heat capacity variations in the temperature range of the experiment can be neglected. Its value in this experiment is equal to ( $C = 4.1813 \frac{kJ}{kg.K}$ ) [27]. It should also be noted that:

$$\dot{m} = \rho \cdot Q = \rho \cdot \alpha \cdot rpm \tag{8}$$

In Fig. 14, the diagram of the fluid inlet and outlet temperature difference ( $\Delta T = T_{out} - T_{in}$ ) against rpm (flow rate) for two types of copper and aluminum serpentine tubes is drawn at radiation intensity of  $G = 1000 \frac{W}{m^2}$ . The results indicated that as the number of pump rounds or the fluid flow rate, increases, the temperature difference would diminish and, in particular under similar conditions, the temperature difference achieved from the copper serpentine tubes will be greater than the aluminum tubes which can again be attributed to the higher thermal conductivity of copper.

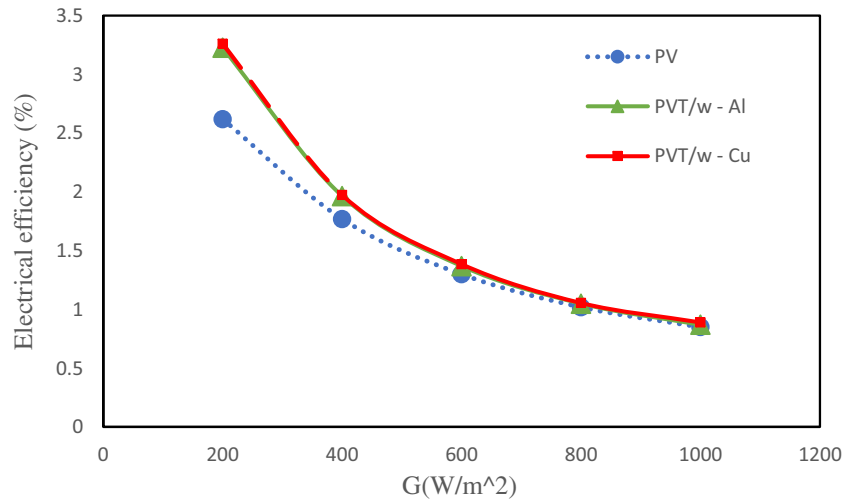
In Fig. 15 the inlet and outlet temperature differences during varying pump speeds are plotted. The effect of varying incoming radiation as well as tube material is included as well. A similar trend (in comparison with Fig. 14) is evident, however, at lower radiation intensities, because of the lower energy input, the temperature difference will be narrower. By comparing aluminum and copper tubes, it can be derived that at identical radiation levels, the copper tube exhibited a slightly higher temperature difference and as a result, a better performance. Nevertheless, since aluminum is much cheaper than copper and the temperature difference is not remarkable, using an aluminum tube is recommended. Moreover, it can be deduced from Fig. 15 that there is a gap between  $\Delta T$  at radiation levels of  $200 \frac{W}{m^2}$  and  $400 \frac{W}{m^2}$  which will be diminished at higher levels. The reason behind this phenomenon is due to the conversion rate of the incoming radiation into electricity. At lower radiation levels, most of the incident radiation is converted since the electrical efficiency of thin films is less than 7%. However, at higher radiation levels, only about 3–5% of the incoming radiation is converted into electrical energy and the rest of it is absorbed as thermal energy.

By calculating the temperature difference between the fluid inlet and outlet, the thermal efficiency of the PVT/w system with copper and aluminum tubes in accordance with eq. (2) can be calculated at different radiation intensities and various pump rounds (different flow rates). The values obtained for the thermal efficiency are shown in Table 2.

It can be interpreted from Table 2, that in contrast to electrical efficiency, using amorphous modules in the PVT/w



**Fig. 13** The electrical efficiency curves in terms of radiation intensity for the PVT/w system with copper and aluminum tubes and photovoltaic modules (PV)



system make it feasible to achieve high thermal efficiency. Under the same conditions, using copper tubes will result in more thermal efficiency, but since the overall efficiency difference between copper and aluminum tubes are close to each other, aluminum tubes can be applied to save money. According to Table 2., at lower radiation intensity, the thermal efficiency is relatively high but at high radiation intensities the thermal efficiency will be reduced. Another important point is that as the flow rate increases, the thermal efficiency will increase substantially. However, in practical applications, the increase of flow rate will cause an increase in the system’s cost.

Since the use of nanofluids will change the physical properties of the base fluid; there are several empirical equations to obtain the density and specific heat capacity of a nanofluid. Most of these equations are different for any particular nanofluid and are used under certain conditions [28, 29]. Since the fluids physical properties have great theoretical concepts, the use of theoretical methods can be very effective. In this case, eq. (2) can be rewritten as follows:

$$\eta_{th} = \frac{\rho_{eff} \times \alpha \times rpm \times C_{eff} \times (T_{out} - T_{in})}{G \times A_c} \tag{9}$$

where the effective nanofluid thermophysical properties can be obtained as follows [30]:

$$\rho_{eff} = \left(\frac{m}{v}\right)_{eff} = \frac{m_f + m_p}{v_f + v_p} = \frac{\rho_f V_f + \rho_p V_p}{V_f + V_p} = (1 - \phi_p)\rho_f + \phi_p\rho_p \tag{10}$$

$$\phi_p = \frac{V_p}{V_f + V_p} \tag{11}$$

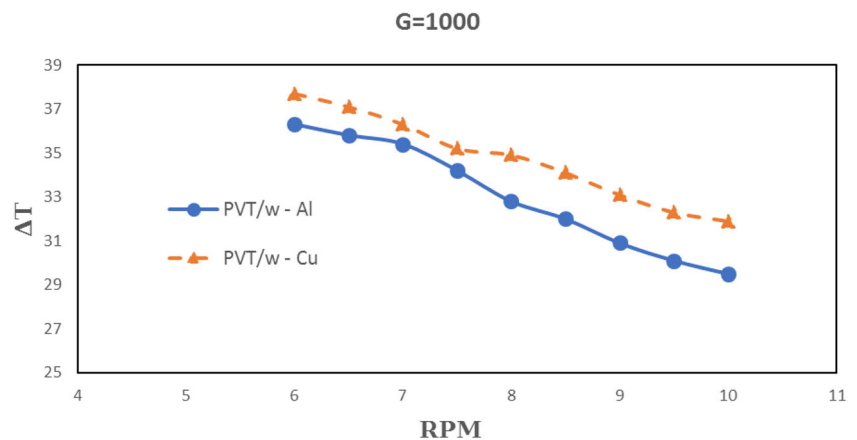
$$C_{eff} = \frac{(1 - \phi_p)\rho_f C_f + \phi_p\rho_p C_p}{\rho_{eff}} \tag{12}$$

$$k_{eff} = \frac{k_p + 2k_f + 2(k_p - k_f)\phi_p k_f}{k_p + 2k_f - (k_p - k_f)\phi_p} \tag{13}$$

In all equations, the subscript “f” represents the base fluid and the subscript “p” is related to the nanoparticle. From eqs. (10) to (12), the density and specific heat capacity of a mixture of nanoparticles with water can be calculated [23]. The values obtained for density are:

$$\begin{aligned} (\rho_{eff})_{TiO_2-H_2O} &= 1003.4815 \text{ gr/l}, (\rho_{eff})_{SiO_2-H_2O} \\ &= 1001.1948 \text{ gr/l}, (\rho_{eff})_{C-H_2O} = 1001.2394 \text{ gr/l} \end{aligned} \tag{14}$$

**Fig. 14** The temperature difference curves in terms of the number of pump rounds for PVT/w system with copper and aluminum tubes



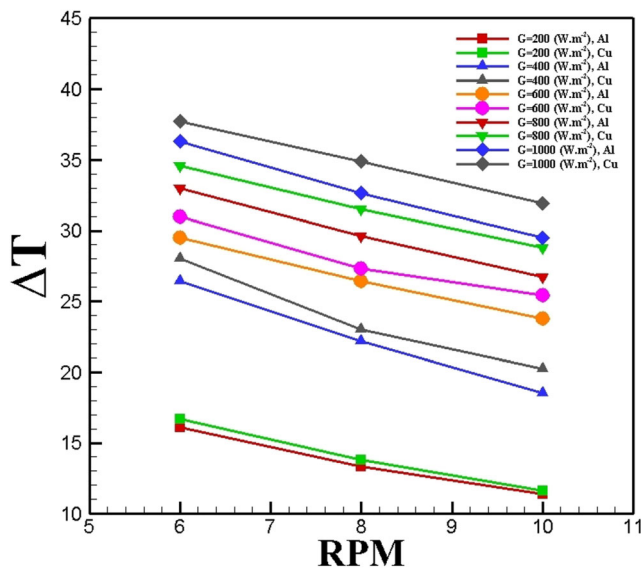


**Fig. 15** The temperature difference lines against various pump speeds at different solar intensities

As it is known, the density of the nanofluid will be slightly higher than the pure water. Then the specific heat capacity values will be obtained as follows:

$$\begin{aligned} (C_{eff})_{TiO_2-H_2O} &= 4.1656 \frac{kJ}{kg.K}, (C_{eff})_{SiO_2-H_2O} \\ &= 4.1737 \frac{kJ}{kg.K}, (C_{eff})_{C-H_2O} = 4.1736 \frac{kJ}{kg.K} \end{aligned} \quad (15)$$

The specific heat capacity of nanofluids will be slightly reduced compared to pure water.

Numerous theories exist to calculate the effective thermal conductivity of liquid-solid suspensions. Each of them considers specific parameters with a limited range that affect the thermal conductivity of nanofluids. These parameters are known as particle concentration, particles size, particle shape, temperature, sonication, etc. Since there is no unit and reliable formula to cover the effect of the whole parameters effect on the effective thermal conductivity, in this study it has been

tried to use the Maxwell static model which is suitable for mono-disperse, low volume-fraction mixtures of spherical shaped nanoparticles (eq. 13) [31]. Table 3. provides information related to thermal conductivity of base fluid (water) and nanoparticles used in this study [32]. It is noteworthy to mention that by using eq. 13, the surfactant's effect on thermal conductivity of nanofluid will not be considered which is a reasonable assumption at a low volume-fraction mixture of nanoparticles [33].

In Fig. 16, the effect of different types of nanofluids at the radiation intensity of  $G = 1000 \frac{W}{m^2}$  for a copper tube is shown.

As shown in Fig. 16, the addition of nanofluid to the system can significantly increase the difference in temperature of the inlet and outlet and thus increase the thermal efficiency. Among the three types of nanofluids ( $C-H_2O$ ,  $TiO_2-H_2O$  and  $SiO_2-H_2O$ ) with 0.1% concentration used in this experiment, the graphite nanofluid mixture ( $C-H_2O$ ) showed the best performance. Now, by using eq. (9), the thermal efficiency of the PVT/w system with different nanofluids could be calculated. PVT/w systems using nanofluids have higher thermal efficiency compared to pure fluid. In this experiment, Graphite nanofluid ( $C-H_2O$ ),  $TiO_2-H_2O$  nanofluid and  $SiO_2-H_2O$  nanofluid increased the relative thermal efficiency of the system (compared to the PVT/w system without nanofluid) approximately 24.15%, 21.4% and 15.73% respectively.

## Uncertainty Analysis

Uncertainty analysis for the experimental results of this study can be divided into two categories; uncertainty in the direct measurement of independent parameters and uncertainty in the results determined from dependent parameters. The first category of uncertainties is evaluated by repeating each experiment for at least 3 times and calculating the standard deviation. In Fig. 17, repeated experiments on the achievement of the I-V curve are

**Table 2** PVT/w system thermal efficiency with “Al” and “Cu” tubes at different flow rates and radiation intensities

	$G = 200 \frac{W}{m^2}$		$G = 400 \frac{W}{m^2}$		$G = 600 \frac{W}{m^2}$		$G = 800 \frac{W}{m^2}$		$G = 1000 \frac{W}{m^2}$	
	Al	Cu	Al	Cu	Al	Cu	Al	Cu	Al	Cu
6 rpm	74.2%	76.97%	60.84%	64.52%	45.32%	47.62%	38.02%	39.86%	33.46%	34.75%
8 rpm	81.73%	84.8%	68.21%	70.67%	54.08%	55.92%	45.47%	48.39%	40.06%	42.89%
10 rpm	87.57%	89.11%	71.05%	77.58%	60.94%	65.04%	51.27%	55.31%	45.32%	49.01%

**Table 3** Thermal conductivities of solid particles and water as working fluid

	Water	C (graphite)	SiO <sub>2</sub>	TiO <sub>2</sub>
<b>Thermal conductivity</b>	0.6	2000	1.3	8.37
<b>Effective thermal conductivity of nanofluid</b> ( $\phi=0.1\%$ )	–	0.6018	0.6005	0.6014

shown at an intensity of  $G = 1000 \frac{W}{m^2}$ , proving that I-V curves do not differ from each other. Moreover, in Fig. 18, the values of the fluid inlet and outlet temperature difference of the aluminum tube, are shown in terms of pump rounds ( $Q = \alpha \cdot rpm$ ), at a radiation intensity of  $G = 1000 \frac{W}{m^2}$ . The diagrams are very close to each other. As a result, the tests are reasonably accurate in terms of repeatability.

The second category is determined by utilizing the Taylor series method for the propagation of uncertainties [34]. In this method, the uncertainty of independent parameters such as open-circuit voltage, short circuit current, and the temperature difference can be calculated via the below eq. (16).

$$S_x = \left[ \frac{1}{N-1} \sum_{i=1}^N (X_i - \bar{X})^2 \right]^{1/2} \tag{16}$$

In the eq. (16),  $\bar{X}$  is obtained as follows:

$$\bar{X} = \frac{1}{N} \sum_{i=1}^N X_i \tag{17}$$

The maximum uncertainty percentage of open-circuit voltage, short circuit current, and the temperature difference are  $\pm 3.27\%$ ,  $\pm 3.74\%$ , and  $\pm 0.87\%$  respectively.

The uncertainty of the dependent parameters such as power in the Taylor series method can be calculated by eq. (18):

$$U_r = \left[ \left( \frac{\partial r}{\partial X_1} U_{X_1} \right)^2 + \left( \frac{\partial r}{\partial X_2} U_{X_2} \right)^2 + \dots + \left( \frac{\partial r}{\partial X_j} U_{X_j} \right)^2 \right]^{1/2} \tag{18}$$

By using eqs. (16–18), the maximum uncertainty percentage for power, electrical and thermal efficiencies can be obtained as  $\pm 3.75\%$ ,  $\pm 3.75\%$ , and  $\pm 0.87\%$  respectively. The calculated values of uncertainties demonstrate the reliability of the obtained experimental results.

### Conclusion

In the present study, a photovoltaic-thermal hybrid system with water fluid (PVT/w) was investigated. By performing various experiments, the electrical and thermal efficiency of the system under different conditions have been investigated. Furthermore, to examine the significance of nanofluids, respective results contingent upon the presence of nanoparticles have been presented and compared. The results demonstrated that since amorphous modules have a very low electrical efficiency, employing

**Fig. 16** The temperature difference curves in terms of the pump rounds for the PVT/w system with copper tubes and various nanofluids

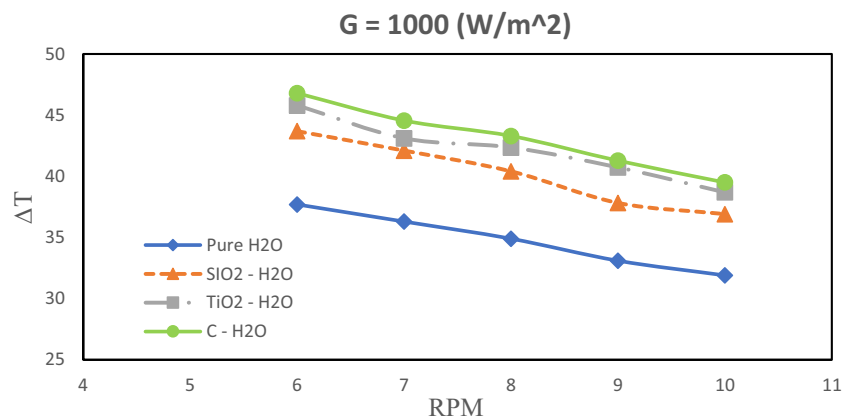
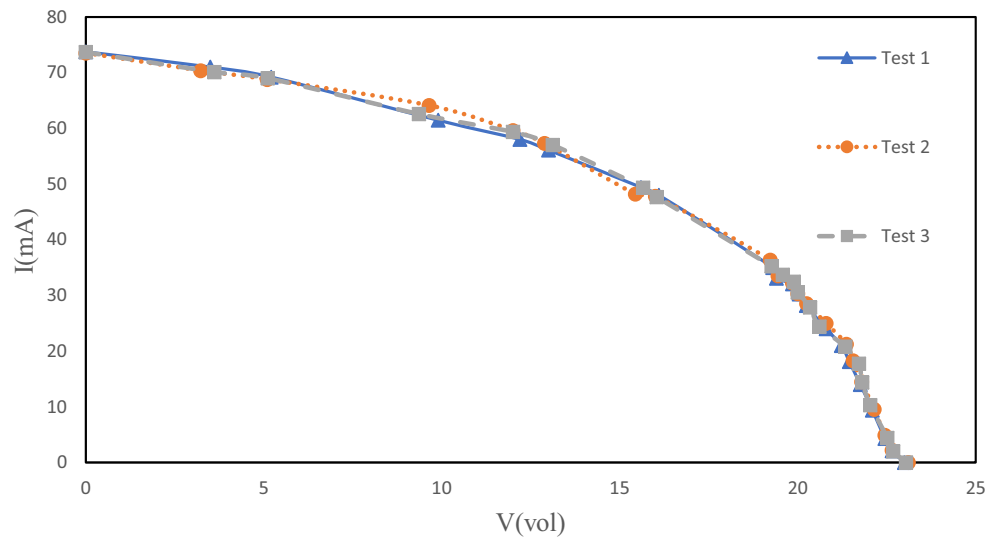


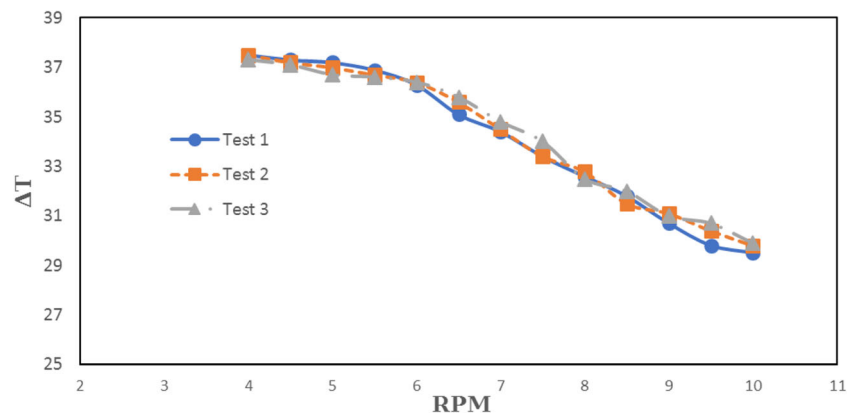
**Fig. 17** I-V curves of different tests at  $G = 1000 \frac{W}{m^2}$



a PVT/w system can elevate their electrical efficiency up to nearly 0.6%. Moreover, amorphous photovoltaic systems are economically cheap and the lost energy in the electrical field could be captured by thermal fluid flow. Applying copper tubes in comparison to aluminum tubes will give us more thermal efficiency. The best result for the copper tube and aluminum tube is 89.11% and 87.57% respectively at  $200 \text{ W/m}^2$  radiation intensity. Since their thermal efficiency is close to each other, aluminum can be used to economically save money. The use of nanofluid can increase the thermal efficiency of the system, but this is costly and the nanofluid stability problem needs to be considered during long-term applications. C,  $\text{TiO}_2$  and  $\text{SiO}_2$  nanoparticles dispersed in water-based nanofluids increased the thermal efficiency of

the system (compared to the PVT/w system without nanofluid) by approximately 24.15%, 21.4%, and 15.73% respectively. Not only the thermal efficiency of the PVT/w system is increased by using nanofluid, but also the electrical efficiency is increased as well. This is because of the fact that the higher the PVT systems' temperature, the lower their performance will be, therefore, since nanofluids are more effective in cooling the system, they will help the photovoltaic modules to work at a higher efficiency. The results obtained based on this article are helpful to researchers in the field of photovoltaic-thermal systems and are very useful in designing serpentine tube-plate types of PVT/w systems in areas that are strongly in need of lower-cost thermal collector systems, since the serpentine tube-plate design is economically reliable.

**Fig. 18**  $\Delta T - rpm$  tests for a PVT/w system with "Al" tubes at  $G = 1000 \frac{W}{m^2}$





**Nomenclature**  $A_c$ , Photovoltaic module area ( $cm^2$ );  $C$ , Specific heat capacity ( $kJ \cdot kg^{-1} \cdot K^{-1}$ );  $G$ , Solar radiation intensity ( $W \cdot m^{-2}$ );  $I_{sc}$ , Short circuit current ( $mA$ );  $I_{MP}$ , Current at the maximum power point ( $mA$ );  $k$ , Thermal conductivity ( $W \cdot m^{-1} \cdot K^{-1}$ );  $\dot{m}$ , Mass flow rate ( $kg \cdot s^{-1}$ );  $P_{PV}$ , Photovoltaic module power ( $W$ );  $P_{MP}$ , Maximum power ( $W$ );  $Q$ , Volumetric flow rate ( $m^3 \cdot s^{-1}$ );  $rpm$ , Peristaltic pump round per minute;  $T_{in}$ , Inlet fluid temperature ( $^{\circ}C$ );  $T_{out}$ , Outlet fluid temperature ( $^{\circ}C$ );  $\Delta T$ , Temperature difference ( $^{\circ}C$ );  $V_{oc}$ , Open circuit voltage ( $V$ );  $V_{MP}$ , Voltage at the maximum power point ( $V$ )

**Greek symbols**  $\alpha$ , Peristaltic pump specific measurement coefficient ( $ml \cdot s^{-1} \cdot rpm^{-1}$ );  $\rho$ , Density ( $kg \cdot m^{-3}$ );  $\eta_e$ , Electrical efficiency;  $\eta_{th}$ , Thermal efficiency;  $\eta_{tot}$ , Total efficiency;  $\phi$ , Nanofluid concentration

**Subscripts**  $bf$ , Base fluid;  $eff$ , effective coefficient (for nanofluids)

## Declarations

**Conflict of Interests** No conflict of interest exists in the submission of this manuscript, and manuscript is approved by all authors for publication. I would like to declare on behalf of my co-authors that the work described was original research that has not been published previously, and is not under consideration for publication elsewhere, in whole or in part. All the authors listed have approved the manuscript that is enclosed.

## References

- Omubo-Pepple V, Israel-Cookey C, Alaminokuma G (2009) Effects of temperature, solar flux and relative humidity on the efficient conversion of solar energy to electricity. *Eur J Sci Res* 35(2):173–180
- Berginc M et al (2007) The effect of temperature on the performance of dye-sensitized solar modules based on a propyl-methylimidazolium iodide electrolyte. *Solar energy materials and solar modules* 91(9):821–828
- Radziemska E (2009) Performance analysis of a photovoltaic-thermal integrated system. *International Journal of Photoenergy* 2009
- Wolf M (1976) Performance analyses of combined heating and photovoltaic power systems for residences. *Energy Conversion* 16(1–2):79–90
- Florschuetz L (1979) Extension of the Hottel-Whillier model to the analysis of combined photovoltaic/thermal flat plate collectors. *Sol Energy* 22(4):361–366
- Prakash J (1994) Transient analysis of a photovoltaic-thermal solar collector for co-generation of electricity and hot air/water. *Energy Convers Manag* 35(11):967–972
- Tripanagnostopoulos Y et al (2002) Hybrid photovoltaic/thermal solar systems. *Sol Energy* 72(3):217–234
- Zondag HA et al (2002) The thermal and electrical yield of a PV-thermal collector. *Sol Energy* 72(2):113–128
- Zondag H et al (2003) The yield of different combined PV-thermal collector designs. *Sol Energy* 74(3):253–269
- Tiwari A et al (2009) Exergy analysis of integrated photovoltaic thermal solar water heater under constant flow rate and constant collection temperature modes. *Appl Energy* 86(12):2592–2597
- Kalogirou SA (2001) Use of TRNSYS for modelling and simulation of a hybrid pv-thermal solar system for Cyprus. *Renew Energy* 23(2):247–260
- Kalogirou SA, Tripanagnostopoulos Y (2006) Hybrid PV/T solar systems for domestic hot water and electricity production. *Energy Convers Manag* 47(18–19):3368–3382
- Chow TT et al (2010) Potential use of photovoltaic-integrated solar heat pump system in Hong Kong. *Appl Therm Eng* 30(8–9):1066–1072
- Gupta, S.K. and S. Pradhan, A review of recent advances and the role of nanofluid in solar photovoltaic thermal (PV/T) system. *Materials Today: Proceedings*, 2020
- Sardarabadi M, Passandideh-Fard M, Heris SZ (2014) Experimental investigation of the effects of silica/water nanofluid on PV/T (photovoltaic thermal units). *Energy* 66:264–272
- Hussien HA, Noman AH, Abdulmunem AR (2015) Indoor investigation for improving the hybrid photovoltaic/thermal system performance using nanofluid (Al<sub>2</sub>O<sub>3</sub>-water). *Eng Tech J* 33(4):889–901
- Michael JJ, Iniyan S (2015) Performance analysis of a copper sheet laminated photovoltaic thermal collector using copper oxide–water nanofluid. *Sol Energy* 119:439–451
- Khanjari Y, Kasaiean A, Pourfayaz F (2017) Evaluating the environmental parameters affecting the performance of photovoltaic thermal system using nanofluid. *Appl Therm Eng* 115:178–187
- Ho C et al (2010) Natural convection heat transfer of alumina-water nanofluid in vertical square enclosures: an experimental study. *Int J Therm Sci* 49(8):1345–1353
- Tripanagnostopoulos Y et al (2005) Energy, cost and LCA results of PV and hybrid PV/T solar systems. *Prog Photovolt Res Appl* 13(3):235–250
- Yu W, Xie H (2012) A review on nanofluids: preparation, stability mechanisms, and applications. *J Nanomater* 2012
- Li Y et al (2009) A review on development of nanofluid preparation and characterization. *Powder Technol* 196(2):89–101
- Ghadimi A, Saidur R, Metselaar H (2011) A review of nanofluid stability properties and characterization in stationary conditions. *Int J Heat Mass Transf* 54(17–18):4051–4068
- Gorji TB, Ranjbar A (2016) A numerical and experimental investigation on the performance of a low-flux direct absorption solar collector (DASC) using graphite, magnetite and silver nanofluids. *Sol Energy* 135:493–505
- Ali N, Teixeira JA, Addali A (2018) A review on nanofluids: fabrication, stability, and thermophysical properties. *J Nanomater* 2018
- Gorji TB, Ranjbar A (2017) Thermal and exergy optimization of a nanofluid-based direct absorption solar collector. *Renew Energy* 106:274–287
- Bergman, T.L., et al., *Introduction to heat transfer*. 2011: John Wiley & Sons
- Pak BC, Cho YI (1998) Hydrodynamic and heat transfer study of dispersed fluids with submicron metallic oxide particles. *Experimental Heat Transfer an International Journal* 11(2):151–170
- Subramanian, K., T.N. Rao, and A. Balakrishnan, *Nanofluids and their engineering applications*. 2019: CRC Press
- Minkowycz, W., E.M. Sparrow, and J.P. Abraham, *Nanoparticle heat transfer and fluid flow*. Vol. 4. 2012: CRC press
- Islam MR, Shabani B, Rosengarten G (2016) Nanofluids to improve the performance of PEM fuel module cooling systems: a theoretical approach. *Appl Energy* 178:660–671
- Chamsa-Ard W et al (2017) Nanofluid types, their synthesis, properties and incorporation in direct solar thermal collectors: a review. *Nanomaterials* 7(6):131
- Das PK et al (2018) Stability and thermophysical measurements of TiO<sub>2</sub> (anatase) nanofluids with different surfactants. *J Mol Liq* 254: 98–107
- Coleman, H.W. and W.G. Steele, *Experimentation, validation, and uncertainty analysis for engineers*. 2018: John Wiley & Sons

**Publisher's Note** Springer Nature remains neutral with regard to jurisdictional claims in published maps and institutional affiliations.

